JOURNAL OF GEOPHYSICAL RESEARCH, VOL. 99, NO. C3, PAGES 5219–5236, MARCH 15, 1994

Correcting infrared satellite estimates of sea surface temperature for atmospheric water vapor attenuation

William J. Emery, Yunyue Yu,[1] and Gary A. Wick
Colorado Center for Astrodynamics Research, University of Colorado, Boulder

Peter Schluessel
Meteorology Institute, University of Hamburg, Hamburg, Germany

Richard W. Reynolds
Climate Analysis Center, National Weather Service, Washington, D.C.

Abstract. A new satellite sea surface temperature (SST) algorithm is developed that uses nearly coincident measurements from the microwave special sensor microwave imager (SSM/I) to correct for atmospheric moisture attenuation of the infrared signal from the advanced very high resolution radiometer (AVHRR). This new SST algorithm is applied to AVHRR imagery from the South Pacific and Norwegian seas, which are then compared with simultaneous in situ (ship based) measurements of both skin and bulk SST. In addition, an SST algorithm using a quadratic product of the difference between the two AVHRR thermal infrared channels is compared with the in situ measurements. While the quadratic formulation provides a considerable improvement over the older cross product (CPSST) and multichannel (MCSST) algorithms, the SSM/I corrected SST (called the water vapor or WVSST) shows overall smaller errors when compared to both the skin and bulk in situ SST observations. Applied to individual AVHRR images, the WVSST reveals an SST difference pattern (CPSST-WVSST) similar in shape to the water vapor structure while the CPSST-quadratic SST difference appears unrelated in pattern to the nearly coincident water vapor pattern. An application of the WVSST to week-long composites of global area coverage (GAC) AVHRR data demonstrates again the manner in which the WVSST corrects the AVHRR for atmospheric moisture attenuation. By comparison the quadratic SST method underestimates the SST corrections in the lower latitudes and overestimates the SST in the higher latitudes. Correlations between the AVHRR thermal channel differences and the SSM/I water vapor demonstrate the inability of the channel difference to represent water vapor in the midlatitude and high latitudes during summer. Compared against drifting buoy data the WVSST and the quadratic SST both exhibit the same general behavior with relatively small differences with the buoy temperatures.

Introduction

The largest error source in the computation of sea surface temperature (SST) from infrared satellite imagery is the correction for signal attenuation by atmospheric water vapor. The multichannel SST (MCSST) algorithm [*McClain et al.*, 1985] used a linear difference between two different thermal infrared channels to correct for this atmospheric moisture effect by the differential absorption in the two channels [*McMillin and Crosby*, 1984; *McClain et al.*, 1985]. A further improvement in water vapor correction was later introduced by *Walton* [1988] and *Walton et al.* [1990] which was called the cross product SST (CPSST). Using a nonlinear formulation, the CPSST was designed to improve the water vapor correction to SST in the moisture laden tropics. In both the CPSST and the former MCSST the algorithm coefficients are derived by matchups with in situ buoy SST measurements.

[1]Permanent affiliation at Ocean University of Qingdao, Qingdao, Peoples Republic of China.

Paper number 93JC03215.
0148-0227/94/93JC-03215$05.00

As discussed by *Maul and Sidran* [1973] and *Hagan* [1989], it is necessary to have three independent measurements to accurately compute SST. Here the problem is specifying both the SST and its atmospheric correction. *Maul and Sidran* [1973] suggested that three thermal infrared channels be used to compute SST. Others (I. Barton, personal communication, 1993) have suggested that these three independent measurements should be of water leaving radiance, the atmospheric temperature profile, and the atmospheric water vapor profile. In the case of the MCSST and the CPSST, the water vapor effect is incorporated into the differential absorption of the two infrared channels as represented by the difference between the two thermal infrared brightness temperatures. Since the important information is how much the atmospheric moisture column of interest varies from the norm, we require some measurement of the total column moisture to correct the infrared SST. Since we do not have accurate coincident measures of the atmospheric water vapor profile, we will instead use a satellite-based estimate of total column atmospheric water vapor.

In this paper we will introduce an SST algorithm that employs measurements of total column atmospheric water vapor from nearly coincident special sensor microwave imager (SSM/I) data for advanced very high resolution radiometer (AVHRR) SST correction. Since the SSM/I and AVHRR are both carried by spacecraft in Sun-synchronous polar orbits of similar altitude, they have similar pass times over most areas. Since we used SSM/I data from a period where only one instrument was operating, we used water vapor averages over 2 days to compute the atmospheric moisture content. A similar algorithm, which adds the square of the difference between AVHRR channels 4 and 5 (called here the quadratic method) to the traditional MCSST, was suggested to us by I. Barton (personal communication, 1993). In this approach the assumption is made that the atmospheric moisture content can be estimated from the difference between channels 4 and 5 and added as a square to the linear correction. This approach will be compared with the SST algorithm using the SSM/I corrections (called the water vapor or WVSST) and the standard CPSST and MCSST algorithms. Both the new WVSST and the quadratic SST will be derived as skin surface temperature algorithms using radiative transfer computations from a suite of global radiosonde profiles. For these algorithms, both ideal (noise) and specified instrument noise level simulations were carried out. This is in contrast to the operational practice of computing the SST algorithm coefficients by matchups with in situ drifting buoy SST measurements. Simulations were also performed using the same radiosonde data set and radiative transfer code to derive new coefficients for the CPSST and the MCSST. The results of the simulations are then used to compare the accuracy of all of the algorithms when derived from a common basis.

All SST algorithms will then be applied to AVHRR images from the South Pacific and the Norwegian seas that were collected coincident with in situ measurements of skin and bulk SSTs from research vessels. For these comparisons the operational CPSST and MCSST algorithms are used rather than the algorithms derived in the simulations discussed above. This was done because the operational algorithms were considered the more appropriate for our application to real data. The satellite based SSTs for all algorithms will be intercompared and will be compared with the simultaneous skin and bulk SST measurements. Even with the limitations of cloud cover in many of these AVHRR data sets there is a substantial amount of data with which to evaluate the performance of the various SST algorithms.

Finally, to demonstrate the global character of the relationships between these algorithms, we used global area coverage (GAC) AVHRR data to form global SST maps. We used two 1-week periods in May-June 1990 when both AVHRR and SSM/I data were readily available. We have also compared SSTs from global drifting buoy data with our satellite-based SST estimates. While we will only present 1 week's results, both weeks displayed very similar behavior in terms of the performance of the SST algorithms.

Water Vapor SST (WVSST)

In previous studies [*Schluessel et al.,* 1987, 1990; *Wick et al.,* 1992] we made an effort to demonstrate the importance of considering the infrared signal received by the AVHRR as being emitted from the skin layer of the sea surface. In all of these studies, no explicit effort was expended to correct the infrared SST for signal attenuation due to atmospheric moisture. We recognize the importance of this water vapor contamination in our comparisons, and the present study examines a variety of new techniques for correcting the multichannel AVHRR data for atmospheric water vapor attenuation of the SST signal.

Since the primary atmospheric contamination effect on the infrared AVHRR signal is due to total column atmospheric water vapor, we sought additional information to correct the AVHRR data. Having earlier developed a simple linear algorithm for the calculation of water vapor from microwave satellite data from the special sensor microwave imager (SSM/I [*Schluessel and Emery,* 1990]) we decided to explore the correction of the AVHRR SST using water vapor from nearly coincident SSM/I data. The SSM/I and AVHRR are carried by two different Sun-synchronous, polar-orbiting weather satellites, and the data are not absolutely coincident but are not separated by much more than a day. We used 2-day composites from the SSM/I on the Defense Meteorological Satellite Program (DMSP) satellite F8 in order to correct the AVHRR images. An earlier study by *Emery et al.* [1990] demonstrated that the atmospheric moisture field is well represented by a 2- to 4-day composite except for the regions of strong weather fronts.

This new approach to computing infrared AVHRR SST can be derived following the MCSST derivation by

McMillin and Crosby [1984] and making alterations in the atmospheric absorption assumptions. The standard MCSST algorithm can be written as

$$SST = a_1 + a_2 T_4 + \gamma(T_4 - T_5) \quad (1)$$

where T_4 and T_5 are satellite brightness temperatures in channels 4 and 5, respectively, and a_1, a_2 and γ are constants. Physically, this algorithm implies that an accurate SST can be represented as one of the satellite channels (here channel 4), and the difference between the two thermal infrared channel brightness temperatures, adjusted by a constant. The weighting factor γ in the MCSST equation [*McMillin and Crosby,* 1984] is the dual-channel transmissivity ratio which can be written as

$$\gamma = \frac{1 - \tau_4}{\tau_4 - \tau_5} \quad (2)$$

where $\tau_i = e^{-k_i u}$ $(i = 4, 5)$, k_i are the absorption coefficients, and u represents the absorption amount over the atmospheric path length.

We now wish to consider a second-order solution rather than the first-order linear approximation made in the MCSST derivation. This allows us to introduce an explicit correction term for atmospheric water vapor. Writing our transmissivity as

$$\tau_i = 1 - k_i u + \frac{(k_i u)^2}{2} \quad (3)$$

we find that the weighting factor γ is linearally proportional to the atmospheric path length absorption (Appendix A) and can be expressed as

$$\gamma = a_3' + a_4 u \quad (4)$$

where a_3' and a_4 are constants. We assume that u can be expanded into the atmospheric effects due to water vapor and to other factors (primarily atmospheric aerosols). We further assume that nonwater vapor effects are very small relative to the atmospheric moisture contamination and thus write $u = W$, where W represents the water vapor content to transform (4) into

$$\gamma = a_3 + a_4 W \quad (5)$$

Substituting this into (1), we can write our new water vapor corrected SST (now called the WVSST) as

$$WVSST = a_1 + a_2 T_4 + a_3(T_4 - T_5) + a_4 W(T_4 - T_5) \quad (6)$$

where $W = W_0/cos(\theta)$, W_0 is the total column atmospheric water vapor from the sea surface to the satellite, θ is the satellite scan angle (relative to nadir), and a_i are constant coefficients which can be obtained from matching with some form of measurements. For our study we will follow the examples of *Schluessel et al.* [1987] and *Barton* [1985] which used atmospheric simulations based on a radiative transfer model and a suite of radiosonde profiles to compute SST coefficients for a skin SST algorithm.

An alternate approach to this SST formulation was suggested by I. Barton (personnel communication, 1993) which assumes that $(T_4 - T_5)$ is an estimate of the effect of atmospheric moisture instead of using the SSM/I moisture estimate in equation (6). This is the essence of the linear approximation in the original MCSST as expressed in equation (1). If we now extend this same assumption to our second-order approach we can write our W term, in equations (5) and (6), as $(T_4 - T_5)$, resulting in an SST formulation of

$$quadratic\ \ SST = a_1 + a_2 T_4 + a_3(T_4 - T_5) + a_4(T_4 - T_5)^2 \quad (7)$$

The advantage of this formulation is that there is no need for additional data to estimate the water vapor term (W). Thus equation (7) can be used when only AVHRR data are available, while equation (6) requires SSM/I data in addition to the AVHRR data.

For the WVSST in equation (6) we used nearly coincident SSM/I data to compute total column water vapor using the algorithm described by *Schluessel and Emery* [1990]. Recently, this algorithm was compared with many other SSM/I atmospheric water vapor algorithms and with a suite of radiosonde data by C. L. Norris and W. J. Emery (Comparisons of SSM/I water vapor algorithms, submitted to *Journal of Geophysical Research*, 1994). The conclusion was that the *Schluessel and Emery* [1990] algorithm was as accurate as any of the other algorithms and was much easier to apply due to its inherently linear formulation. Thus it will be used exclusively in this paper. It should also be pointed out, however, that the C. L. Norris and W. J. Emery (submitted manuscript, 1994) comparisons clearly demonstrate that other SSM/I water vapor retrieval methods can be used for accurate estimates of total column water vapor and these other methods would then be expected to yield very similar accuracies to our WVSST when they are used for estimates of W in equations (5) and (6).

Atmospheric Simulations to Compute Algorithm Coefficients

We used the atmospheric transmission model of *Barton* [1985] along with 300 oceanic radiosonde profiles to compute our WVSST and quadratic SST algorithm coefficients. The 300 profiles included the 280 profiles used by *Schluessel et al.* [1987] augmented by approximately 20 profiles from the data set used by *Barton* [1985]. The combined radiosonde data set included data from all latitudes, longitudes, and the winter/summer seasons in the midlatitude and polar latitude. While not completely uniform in distribution, the resulting data set was selected to give the best possible global representation with a limited set of atmospheric profiles. In order to be fair in the comparisons of our new algorithms with the traditional MCSST and CPSST we also used the same atmospheric simulation technique to recom-

Table 1. WVSST Coefficients for NOAA 11 AVHRR

Noise Included			Noise Excluded		
Scan Angle	RMS	Mean	Scan Angle	RMS	Mean
0.0	0.50	0.00	0.0	0.27	0.00
10.0	0.50	-0.01	10.0	0.28	-0.01
20.0	0.52	-0.03	20.0	0.29	-0.03
30.0	0.55	-0.08	30.0	0.33	-0.08
40.0	0.62	-0.17	40.0	0.40	-0.17
50.0	0.78	-0.34	50.0	0.57	-0.37

Algorithm is WVSST $= a_1 + a_2T_4 + a_3(T_4 - T_5) + a_4W_0(T_4 - T_5)/\cos(\theta)$ (K). For noise included, $a_1 = -9.28496$, $a_2 = 1.03676$, $a_3 = 0.68113$, and $a_4 = 0.31748$. For noise excluded, $a_1 = -4.87073$, $a_2 = 1.01984$, $a_3 = 1.45222$, and $a_4 = 0.22798$.

Table 2. Quadratic SST Coefficients for NOAA 11 AVHRR

Noise Included			Noise Excluded		
Scan Angle	RMS	Mean	Scan Angle	RMS	Mean
0.0	0.54	0.00	0.0	0.30	0.00
10.0	0.54	-0.02	10.0	0.30	-0.01
20.0	0.56	-0.07	20.0	0.32	-0.06
30.0	0.62	-0.19	30.0	0.38	-0.15
40.0	0.75	-0.39	40.0	0.53	-0.33
50.0	1.09	-0.80	50.0	0.87	-0.68

Algorithm is quadratic SST $= a_1 + a_2T_4 + a_3(T_4 - T_5) + a_4(T_4 - T_5)^2$ (K). For noise included, $a_1 = -12.56158$, $a_2 = 1.04903$, $a_3 = 0.40598$, and $a_4 = 0.74536$. For noise excluded, $a_1 = -6.03510$, $a_2 = 1.02391$, $a_3 = 1.61243$, and $a_4 = 0.40691$.

pute the coefficients in the two NOAA SST algorithms. Since the operational coefficients were found by comparisons with in situ drifting buoy SST observations, they are necessarily different from our atmospheric simulation coefficients.

In our simulations we used two different assumptions. At first we assumed a perfect instrument with no instrument noise. In order to estimate the effects of instrument noise to our SST calculations we added noise to our simulations equivalent to an estimate of the noise in the satellite radiometers. This noise will influence both the overall error budget and the value of the coefficients since the noise will decrease the covariance used to derive the regression coefficients in the simulations. In addition, when using equation (6), we must also account for the radiometer noise in the SSM/I for estimating the atmospheric water vapor. For our simulations with noise we used a noise level of ± 0.12 K for T_4 and T_5 [*Brown et al.*, 1985] and a noise level of ± 0.54 g/cm^2 for the SSM/I water vapor values [*Schluessel and Emery*, 1990].

The resulting coefficients are listed in Tables 1 (WVSST), 2 (quadratic SST), 3 (CPSST), and 4 (MCSST) for the NOAA 11 satellite. Note that no particular effort has been made to account for the inherent nonlinearity in the sensor calibration [*Brown et al.*, 1993] and the NOAA calibration procedure is applied in all cases to convert engineering units to brightness temperatures. Also Tables 1-4 show the RMS differences between the "true" simulation data set SST and that from the algorithm, given as a function of scan angle for both the noise and noiseless cases. In general, the RMS values are a bit smaller for the WVSST when compared to the quadratic SST. Also the quadratic SST RMS differences increase more with higher scan angle than does the WVSST. Although the differences are not statistically significant, both of these new SST algorithms have smaller RMS differences than the MCSST and CPSST algorithms. The CPSST is slightly better than the MCSST, but the new algorithms show improvements over both the CPSST and the MCSST. Further comparisons with the NOAA 11 operational CPSST and MCSST algorithms yielded slightly poorer results (not shown) in terms of RMS differences.

The simulation results are also presented graphically in Figures 1-4 as differences from the "true" or "real" SST from the simulation data set. The WVSST differences in Figure 1 appear very similar to those for the quadratic SST in Figure 2. Both have a 0°C mean difference and the WVSST RMS difference (0.50°C) is only slightly smaller than the 0.54°C difference for the quadratic SST simulations. This suggests that both approaches should perform about equally well in computing SST in the presence of atmospheric moisture. As will be discussed later, this turns out not to be the case when the quadratic SST algorithm is applied to real AVHRR data.

The CPSST simulations in Figure 3 have a slightly larger spread than those in Figures 1 and 2; the mean of 0.07°C is nonzero, and the RMS of ± 0.57°C is a bit

Table 3. CPSST Coefficients for NOAA 11 AVHRR

Noise Included			Noise Excluded		
Scan Angle	RMS	Mean	Scan Angle	RMS	Mean
0.0	0.57	0.07	0.0	0.36	0.07
10.0	0.57	0.05	10.0	0.37	0.06
20.0	0.58	-0.01	20.0	0.37	0.00
30.0	0.63	-0.14	30.0	0.42	-0.12
40.0	0.77	-0.37	40.0	0.57	-0.33
50.0	0.96	-0.83	50.0	0.87	-0.77

Algorithm is CPSST = $(T_{S5}-T_5)(T_4'-T_5)/(T_{S5}-T_5+T_4'-T_{S4})+T_5$ (K), where $T_{S4} = a_{41}+a_{42}T_4$, $T_{S5} = a_{51}+a_{52}T_5$, and $T_4' = T_4+C$. For noise included, $C = 0.55$ and $a_{41} = -36.55507$, $a_{42} = 1.13647$, $a_{51} = -47.68645$, and $a_{52} = 1.17891$. For noise excluded, $C = 0.45$ and $a_{41} = -36.59504$, $a_{42} = 1.13664$, $a_{51} = -47.45669$, and $a_{52} = 1.17812$. Operational CPSST from "NOAA Polar Orbital Data Users Guide" (1991): CPSST = $(0.19069T_5 - 49.16)(T_4 - T_5 + 0.789)/(0.20524T_5 - 0.17334T_4 - 6.78) + 0.92912T_5 + 0.81(T_4 - T_5)(\sec(\theta) - 1) + 18.97$ (K) for daytime and CPSST = $(0.19596T_5 - 48.61)(T_4 - T_5 + 1.46)/(0.20524T_5 - 0.17334T_4 - 6.11) + 0.95476T_5 + 0.980(T_4 - T_5)(\sec(\theta) - 1) + 9.31$ (K) for nighttime.

Table 4. MCSST Coefficients for NOAA 11 AVHRR

Noise Included			Noise Excluded		
Scan Angle	RMS	Mean	Scan Angle	RMS	Mean
0.0	0.60	0.00	0.0	0.33	0.00
10.0	0.61	-0.02	10.0	0.33	-0.01
20.0	0.63	-0.07	20.0	0.35	-0.06
30.0	0.69	-0.18	30.0	0.41	-0.15
40.0	0.83	-0.38	40.0	0.56	-0.31
50.0	1.16	-0.77	50.0	0.89	-0.65

Algorithm is MCSST = $a_1 + a_2T_4 + a_3(T_4 - T_5)$ (K). For noise included, $a_1 = -9.17974$, $a_2 = 1.03453$, and $a_3 = 2.16272$. For noise excluded, $a_1 = -3.73376$, $a_2 = 1.01415$, and $a_3 = 2.64210$.

larger than either of the other two algorithms. While the mean values should have been 0.0, this was never the case. Finally, the MCSST (Figure 4) has a similar pattern but with a larger spread at the low SST values. This leads to the larger RMS value of 0.60°C in spite of the lower mean difference (0.0°C). It should be noted here that for the simulation results we neglected the scan angle corrections of the operational MCSST and CPSST algorithms. We were unable to define those coefficients that depended on scan angle in the operational algorithms. In the subsequent applications to AVHRR data we used the operational CPSST coefficients that do compensate for scan angle variations. We have included the operational CPSST algorithm and its coefficients in Table 3.

Application to Satellite Imagery

For the purposes of evaluating these different infrared SST algorithms we used a series of calibration data sets collected specifically to test the accuracy of skin and bulk SST methods [*Schluessel et al.*, 1987]. Four data sets were collected in the Norwegian Sea (called the Arctic in Table 5), while two data sets were from the southern Pacific. The Norwegian Sea data were all collected by the German R/V *Valdivia* between 71° and 72°N and 12° – 17°E over the period between February 24 and March 11, 1991. In all of these data sets, in situ skin SST was measured from a radiometer mounted on a ship looking at the ocean ahead of the research vessel's bow wave. In the earlier 1990 data from the South Pacific a PRT-5 radiometer was used to collect the skin SST data during a cruise of the R/V *Malcolm Baldrige*. This was the same system used by *Schluessel et al.* [1990], and its specifics are presented by them.

The Norwegian Sea data were collected with a Heimann KT-4 equipped with a 10-12 μm band-pass filter. The radiometer was again mounted so as to point ahead of the ship's bow wave at Brewster's angle (about 50°). Underway calibration of this radiometer was carried out as described by *Schluessel et al.* [1990] for the PRT-5 system. A well-stirred bucket of seawater came into the radiometer's field of view (FOV) each minute to provide an absolute calibration of the measured bucket temperature (assumed to be well stirred to eliminate the skin effect). The KT-4 measurements were recorded as 10-s means of which we rejected those that were affected by the moving calibration bath at the start and finish of each calibration cycle. The remaining 10-s means are then used to build means over 40-50 s which are then further reduced to 1-min measurements. Spikes were

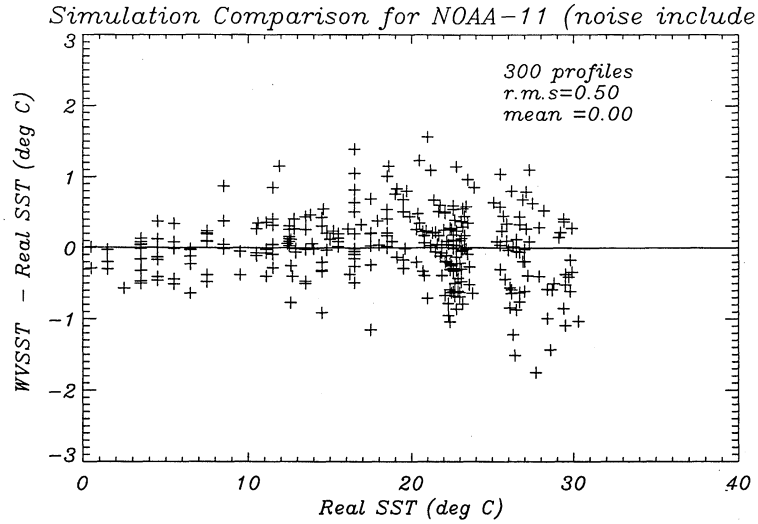

Figure 1. Atmospheric simulation comparison between the WVSST surface temperatures and those from the simulation database.

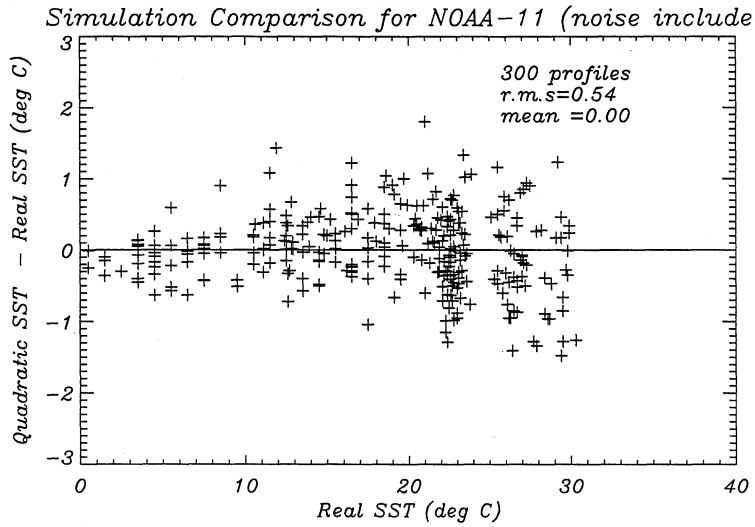

Figure 2. Atmospheric simulation comparison between the quadratic SST surface temperatures and those from the simulation database.

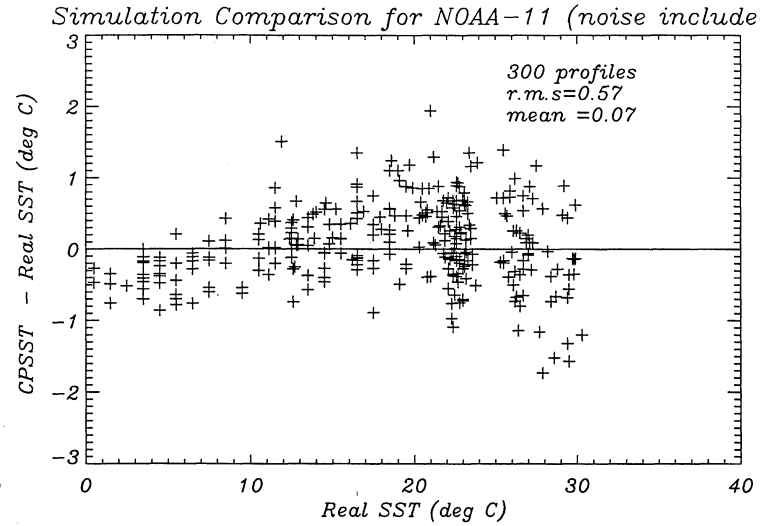

Figure 3. Atmospheric simulation comparison between the CPSST surface temperatures and those from the simulation database.

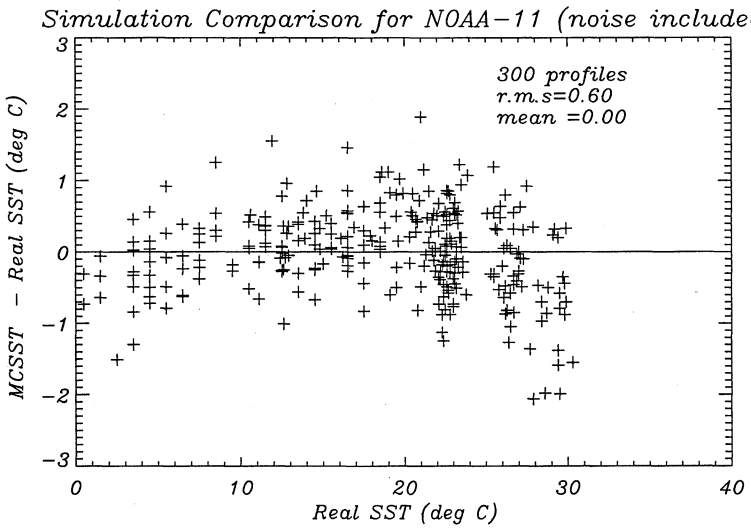

Figure 4. Atmospheric simulation comparison between the MCSST surface temperatures and those from the simulation database.

removed from the series if they deviated more than 0.15 K from the mean of the corresponding measurement cycle. In addition to the KT-4 there were short- and long-wavelength solar insolation instruments and other in situ measurement campaigns that coincided with the collected satellite data.

Similar measurements were made in the South Pacific using the older PRT 5 radiometer. Similar band-pass filters were employed, and the results were generally the same as that for the KT-4. From both the *Valdivia* and from the *Baldrige*, in situ bulk SSTs were measured with the ship's thermosalinograph at a depth of 5 m. This measurement became the basis for the comparisons between bulk and skin SST observations. During these different cruises, AVHRR 1-km high-resolution picture transmission (HRPT) and local area coverage (LAC) data from the NOAA 11 satellite were collected to match the times and locations of the research vessels equipped with skin SST radiometers. Unfortunately, the data from the South Pacific are limited due to both

Table 5. Differences Between AVHRR-SST Estimates and in Situ SST Measurements

	Date	Time, UT	Data Points	Temperature Range, °C	Minus Skin SST				Minus Bulk SST			
					WV	QU	CP	MC	WV	QU	CP	MC
				Arctic Ocean (1991)								
	Feb. 26	1100 (D)	19	5.0-7.0								
Mean					-0.04	0.35	-0.97	-0.39	-0.34	0.45	-1.09	-0.50
RMS					0.38	0.55	1.00	0.45	0.52	0.53	1.11	0.55
	Mar. 6	0240 (N)	98	4.5-7.0								
Mean					-0.39	0.33	-0.72	-0.88	-0.37	0.35	-0.71	-0.85
RMS					0.52	0.48	0.80	0.94	0.45	0.44	0.75	0.89
	Mar. 8	1048 (D)	76	5.0-7.0								
Mean					-0.09	0.08	-0.66	-0.57	0.12	0.17	-0.57	-0.49
RMS					0.45	0.51	0.70	0.63	0.48	0.53	0.67	0.59
	Mar. 9	0206 (N)	134	5.0-7.0								
Mean					-0.17	0.25	-0.45	-0.78	-0.24	0.32	-0.71	-1.00
RMS					0.35	0.44	0.62	0.82	0.41	0.45	0.73	1.03
				South Pacific (1990)								
	Mar. 27	0149 (D)	79	18.5-22.0								
Mean					-0.22	0.26	0.28	0.49	-0.32	0.29	0.33	0.38
RMS					0.51	0.58	0.61	0.62	0.69	0.64	0.68	0.69
	Mar. 28	0138 (D)	139	19.0-22.0								
Mean					-0.39	0.47	0.08	0.32	-0.47	0.49	0.00	0.34
RMS					0.53	0.70	0.36	0.42	0.59	0.67	0.39	0.45

WV, WVSST; QU, quadratic SST; CP, CPSST; MC, MCSST; Mean, mean difference (degrees Celsius); RMS, root mean square difference (degrees Celsius); D, daytime; N, nighttime.

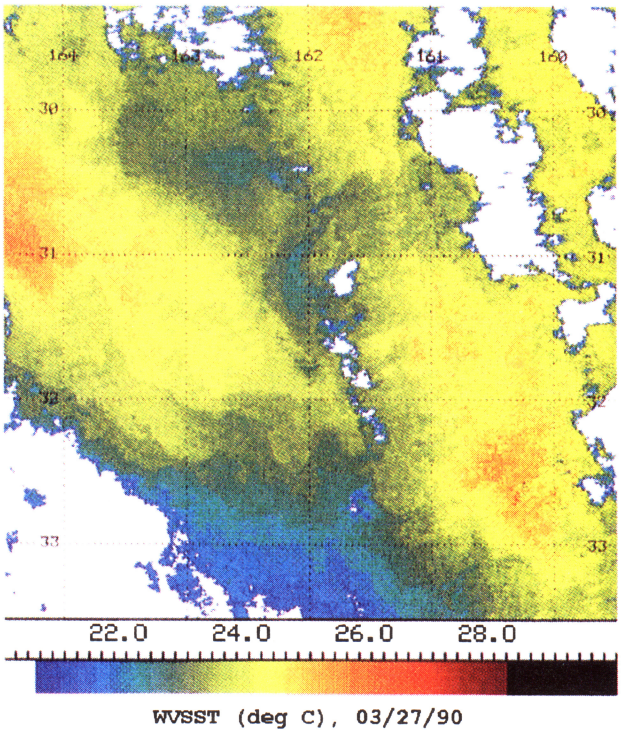

Plate 1. WVSST computed for a single AVHRR image from the South Pacific northeast of New Zealand for March 1990. Clouds are masked as white values and the temperature color scale (degrees Celsius) is given at the bottom of the image.

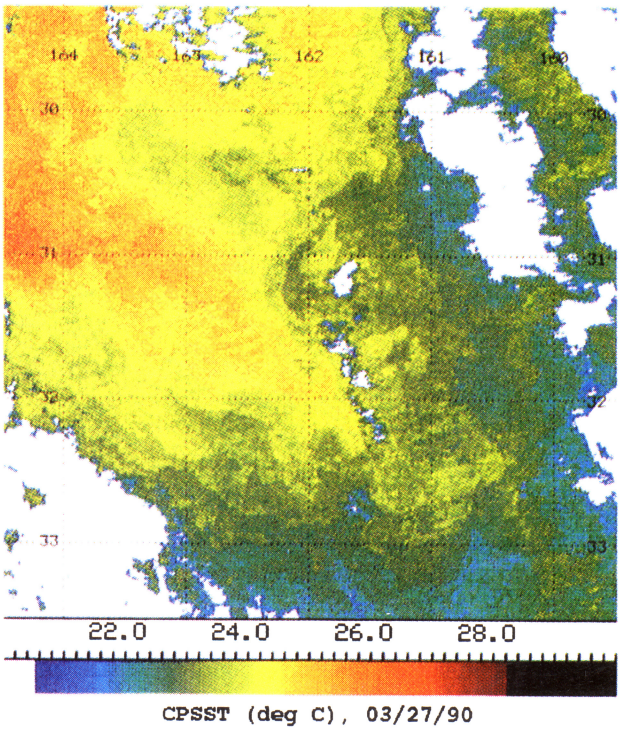

Plate 3. As in Plate 1 for the CPSST.

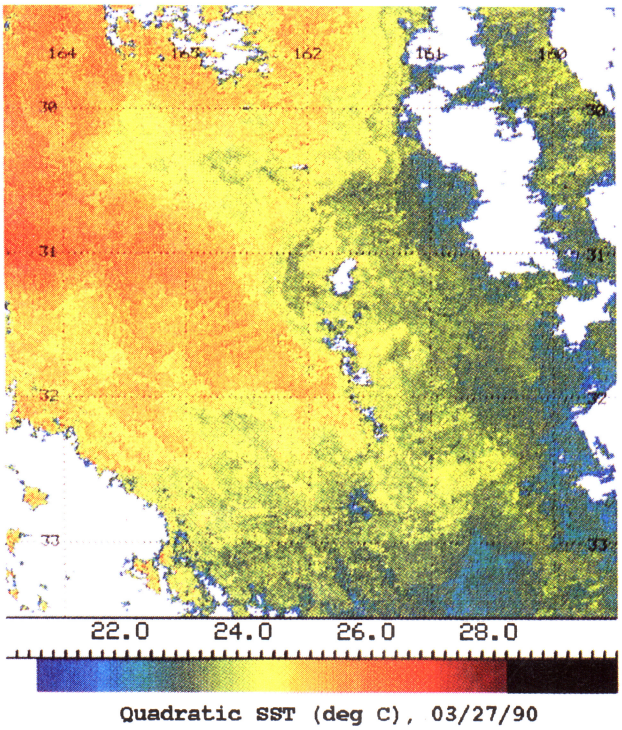

Plate 2. As in Plate 1 for the quadratic SST.

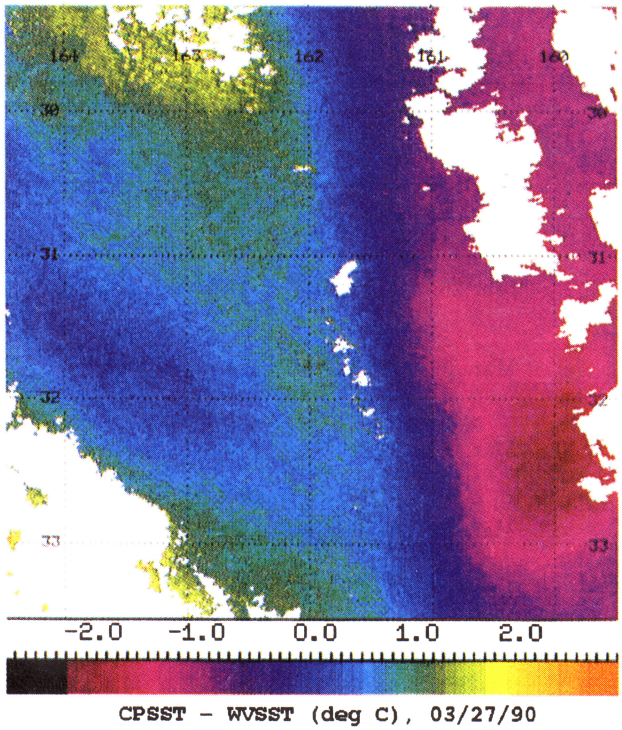

Plate 4. Temperature difference (degrees Celsius) between the CPSST and the WVSST (CPSST-WVSST) for the image in Plate 1.

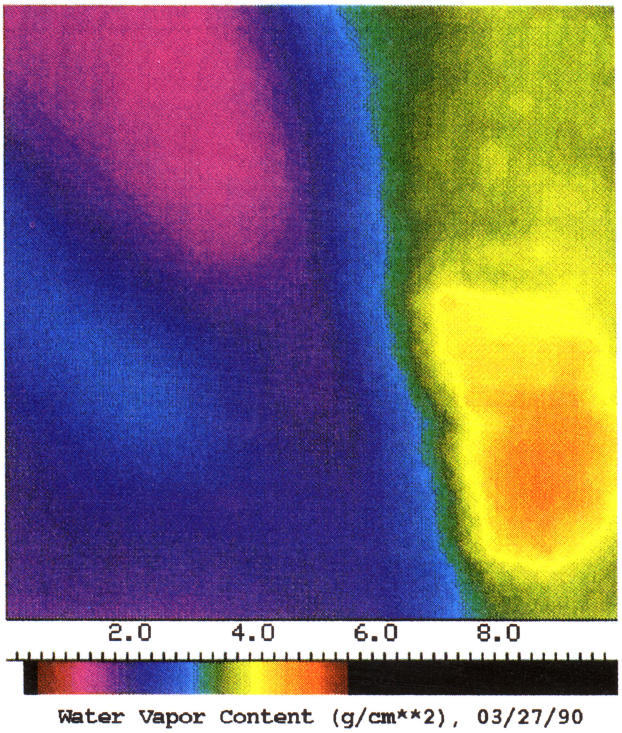

Plate 5. Atmospheric water vapor (grams per square centimeter) computed from SSM/I data from the 2 days surrounding the date and for the area of the image in Plate 1.

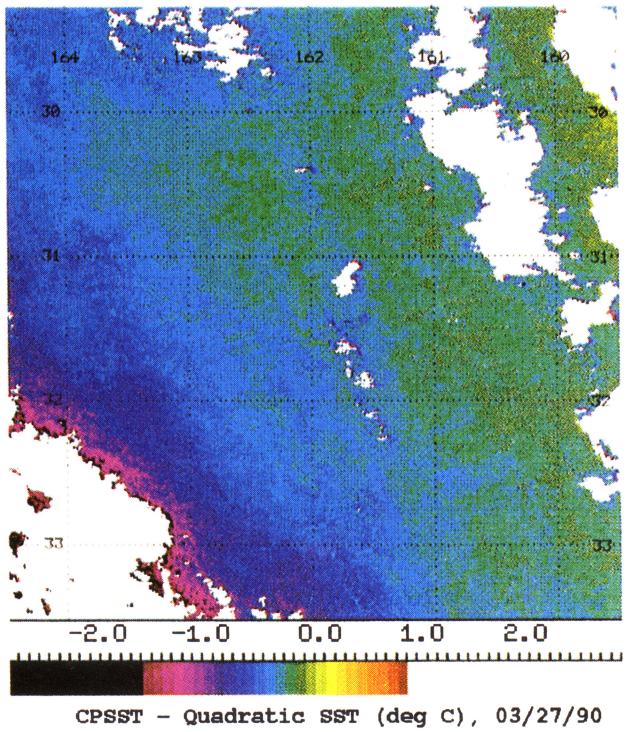

Plate 6. Temperature difference (degrees Celsius) between the CPSST and the quadratic SST (CPSST-quadratic) for the image in Plate 1.

persistent cloud cover and some severe weather that limited the operation of the radiometer absolute calibration reference.

For all of these applications to real AVHRR data, the operational MCSST and CPSST algorithms for NOAA 11 were used rather than the simulated algorithms discussed above. The operational coefficients were taken from *Walton et al.* [1990] and *Kidwell* [1991]. Since the operational algorithms were derived from real data (buoy matchups), we assumed that they would give the best results for our applications.

Plate 1 is an example of the application of the WVSST to an AVHRR image from the midlatitude South Pacific northeast of New Zealand. A similar image for the quadratic SST method is shown in Plate 2. Finally, for comparison, we show the equivalent image for the CPSST method as described above (Plate 3). The overall pattern is similar for all three SST fields, but there are clear differences, as strongly indicated by the lower temperatures in the WVSST image. The warmest general SST pattern is found for the quadratic SST algorithm, while the coolest pattern is for the WVSST. A definite pattern emerges in the difference between the CPSST and the WVSST (Plate 4) which shows a large negative maximum in the southeast corner of this image. A slight positive maximum is found in the northwest with a pocket of nearly 0.0° temperature differences in the central portion of the western part of the image. Comparison with the atmospheric moisture field computed from a 2-day composite of the SSM/I water vapor field (Plate 5) reveals an identical pattern to that for the difference between CPSST and WVSST. A similar difference between the CPSST and the quadratic SST (Plate 6) does not contain the same spatial pattern as seen in Plates 4 and 5. Instead, there is a general eastwest pattern with the far eastern portions of the image having a very slightly negative temperature difference while in the western half of the image the differences are more negative. No pattern of extremes appears in the CPSST-quadratic SST differences (Plate 6). The differences appear to be correlated to the sensor scan angle and could be a result of the larger errors in the quadratic SST at greater scan angles. A similar temperature difference image between the CPSST and the MCSST (not shown) shows almost no difference between these two different split window correction schemes for water vapor contamination.

Looking at these differences in the form of histograms the differences between the CPSST and the WVSST (Figure 5a) clearly indicate the mix of large negative values with smaller positive differences. The negative values result in a secondary peak in the histogram at about -1.2 K, while the primary histogram peak is at a temperature of about 0.6 K. This is consistent with the pattern of maxima seen in Plate 4 which is also apparent in the water vapor pattern of Plate 5. In contrast, the difference histogram for the CPSST-quadratic SST (Figure 5b) has a single peak at about -0.5 K. This is again consistent with the pattern of Plate 6 which shows the dominant value to be slightly negative. The mean difference between the CPSST and the quadratic SST is -0.46 K, while the mean CPSST-WVSST difference is -

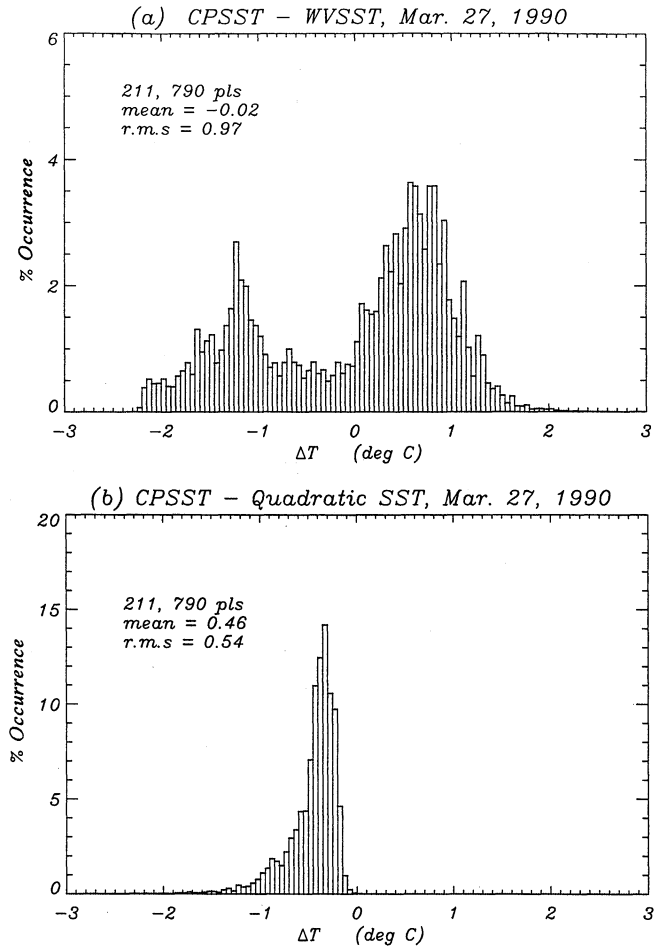

Figure 5. (a) Histogram of the temperature differences in Plate 4. (b) Histogram of the temperature differences in Plate 5.

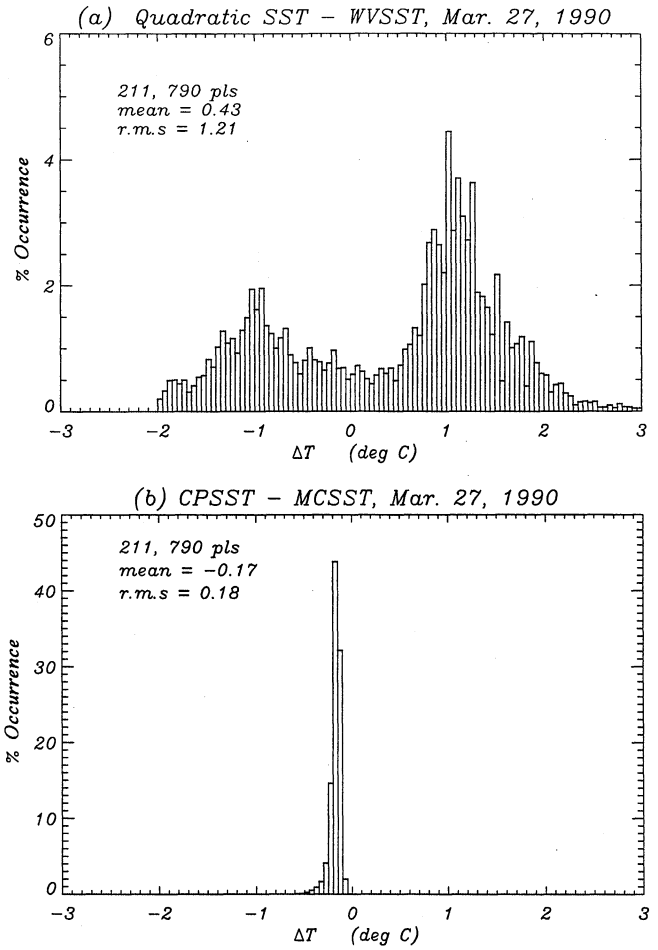

Figure 6. (a) Histogram of the temperature differences between the quadratic SST and the WVSST. (b) Histogram of the temperature differences between the CPSST and the MCSST.

0.02 K. This smaller mean difference is a consequence of the two offsetting peaks in the histogram of Figure 5a. The RMS difference of 0.54 K is much smaller for the CPSST-quadratic SST than the 0.97 K for the CPSST-WVSST due again to the dispersion of the two different peaks in the histogram.

A direct histogram comparison between the quadratic SST and the WVSST for this same image (Figure 6a) also exhibits two distinct peaks corresponding to the peaks in Figure 5a. The primary peak has a center value of about 1.0 K, while the secondary (or smaller) peak is at about -1.0 K. The mean temperature difference is 0.43 K (quadratic SST is warmer as seen in Plate 2) and the RMS difference is 1.21 K. This clearly demonstrates that the two different water vapor correction schemes do not yield the same net result. A histogram comparison between the CPSST and the MCSST (Figure 6b) has a tall peak at about -0.2 K with a very small spread which shows the overall similarity between the CPSST and the MCSST for this particular image. Similar differences were computed for other images in this same region with very similar results.

Numerical Comparisons

Both the mean and RMS differences between the ship-based reference values and the various satellite SST algorithms are presented in Table 5 for various scenes in the Norwegian Sea (Arctic) and South Pacific. In each case the SST algorithms were applied to coincident AVHRR data, and cloud filtering was performed to select only those cases that were not cloud contaminated. Even with the cloud filtering, there is still a significant number of comparison values in each of the cases reported. In Table 5, WV refers to the WVSST, QU refers to the quadratic SST, CP refers to the CPSST, and MC refers to the MCSST. The coefficients from Tables 1 and 2 were used for the WVSST and quadratic SST, respectively, while the operational coefficients were used for the CPSST and the MCSST.

In three out of six cases the mean difference for the WVSST versus the skin SST observations is the smallest for all of the algorithms. In two cases the quadratic SST formula produced the smallest mean difference. In every case the CPSST and MCSST algorithms led to

substantially larger mean differences, except for one of the South Pacific cases. Regarding the RMS differences, the WVSST has the smallest values in four out of the six cases. In terms of RMS differences the values for all of the SST algorithms are much more similar than are the mean differences.

The surprise was that the WVSST differences against the 5-m bulk SST measurements were the smallest for half of the six cases. That the WVSST skin SST algorithm should compare well with the 5-m bulk temperature was not expected. A similar pattern is true for the RMS differences for which three of six minima are for the WVSST. The CPSST and MCSST mean differences are generally much greater than those for the WVSST and the quadratic SST. The RMS values are much more similar in overall magnitude with the CPSST and MCSST having, in general, slightly larger RMS differences. It is interesting to note that for the mean differences the WVSST differences were generally negative, while the quadratic SST formula always produced positive differences. The CPSST and MCSST mean differences were both negative and positive.

The results in Table 5 suggest that against in situ skin SST measurements, the WVSST algorithm is accurate to about 0.2 K in the mean with an RMS variability of about 0.4 K. Likewise against 5-m bulk SST measurements the WVSST algorithm has a mean difference of about -0.40 K with an RMS of 0.5 K. Similar arguments applied to the quadratic SST yield a mean difference of about 0.29 K. An absolute magnitude of the quadratic RMS differences would be much larger than those for the mean. It is surprising that in some cases the CPSST and MCSST mean and RMS differences against the measured skin SST were quite similar to those from the WVSST and the quadratic SST. In general, the CPSST and MCSST algorithms performed worse in the higher-latitude Norwegian Sea applications than they did in the midlatitude South Pacific where they appeared to do as well as the new algorithms in matching both the skin and bulk reference measurements.

Global Comparisons

In order to further test the various satellite SST algorithms we applied them to two individual weeks (only 1 week is presented) of 4 km resolution global area coverage (GAC) AVHRR data. These GAC data were taken from the GAC archive at the National Center for Atmospheric Research (NCAR). To insure that we would have both AVHRR and SSM/I data for our test period, we selected data from the summer of 1990. We composited the GAC AVHRR data over a week long period from May 27 to June 2, 1990. The simple cloud screening algorithm described by *Wick et al.* [1992] was used along with the same image compositing technique. Thus two week-long AVHRR GAC data sets were extracted and processed for application of the various AVHRR SST algorithms.

In addition to the GAC data we also acquired coincident drifting buoy measurements from the Climate Analysis Center (CAC) of the National Weather Service (NWS). Called "superobs" these buoy data were week-long retrievals for grid locations where available on the global ocean. Thus they are consistent in time with the 1-week composites of AVHRR GAC data.

The WVSST, quadratic SST, CPSST, and MCSST global maps computed from the May 27 to June 2, 1990, data (not shown) all appear similar in character. Differences between these SST fields were quite instructive, however. The CPSST-WVSST difference in Plate 7a shows a difference range going from about 0.0 to -2.5 K. Most of the larger negative differences are located in the high atmospheric moisture band of the tropics (white out regions are areas of persistent cloud cover also predominantly located in the tropical ocean and in the high polar latitudes). The corresponding SSM/I water vapor image in Plate 7b clearly indicates this zone of high water vapor in the tropical ocean. Note this image is again a 2-day composite representative of the water vapor during the week. High moisture regions also border some of the continents extending poleward from the tropics. The strong correlation between the global moisture and CPSST-WVSST patterns is consistent with the pattern similarities between Plates 4 and 5 which were the corresponding figures for the sample AVHRR image in the South Pacific.

To test the quadratic SST algorithm, we also used it with the GAC data to compute the global SST difference image in Plate 7c. While a lot of the tropical differences in Plate 7a also appear in Plate 7c, there are sharp magnitude differences at the high polar latitude where the atmospheric moisture content is very low (Plate 7b). When the water vapor amount is low, the quadratic SST produces higher SST values and hence greater negative differences with the CPSST. This is in strong contrast to the WVSST, which does not have negative differences at these higher latitudes. In fact, the CPSST-WVSST differences exhibit a minimum (near zero) at these latitudes in all ocean basins. In addition, the tropical band of negative CPSST-quadratic SST differences is much more fragmented than that in Plate 7a for the WVSST. The continental "halo" effect is dramatically reduced and the core of the tropical difference band appears to have slightly lower magnitudes than were found in Plate 7a.

To better describe the temperature differences between the WVSST and the quadratic SST method, we computed the differences (WVSST-quadratic SST) in Plate 7d. Here positive differences can be found in the tropics, indicating what appears to be an underestimate of the water vapor correction by the quadratic approach. These underestimates also surround many of the low-latitude continental regions where the quadratic SST fails to compensate for the moisture apparent in Plate 7b. At the higher latitudes the differences are mainly negative due to the overestimate of the temperature by the quadratic SST. This problem is more severe

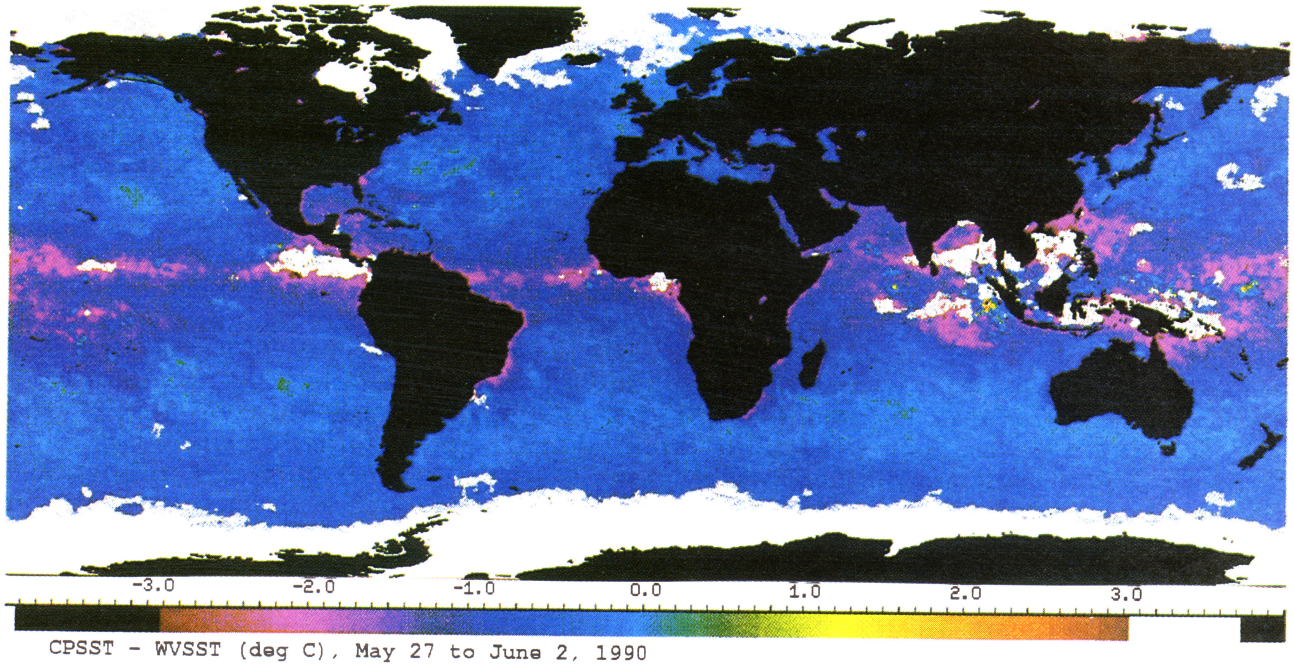

Plate 7a. Global temperature difference (degrees Celsius) between the CPSST and the WVSST (CPSST-WVSST) for May 27 to June 2, 1990.

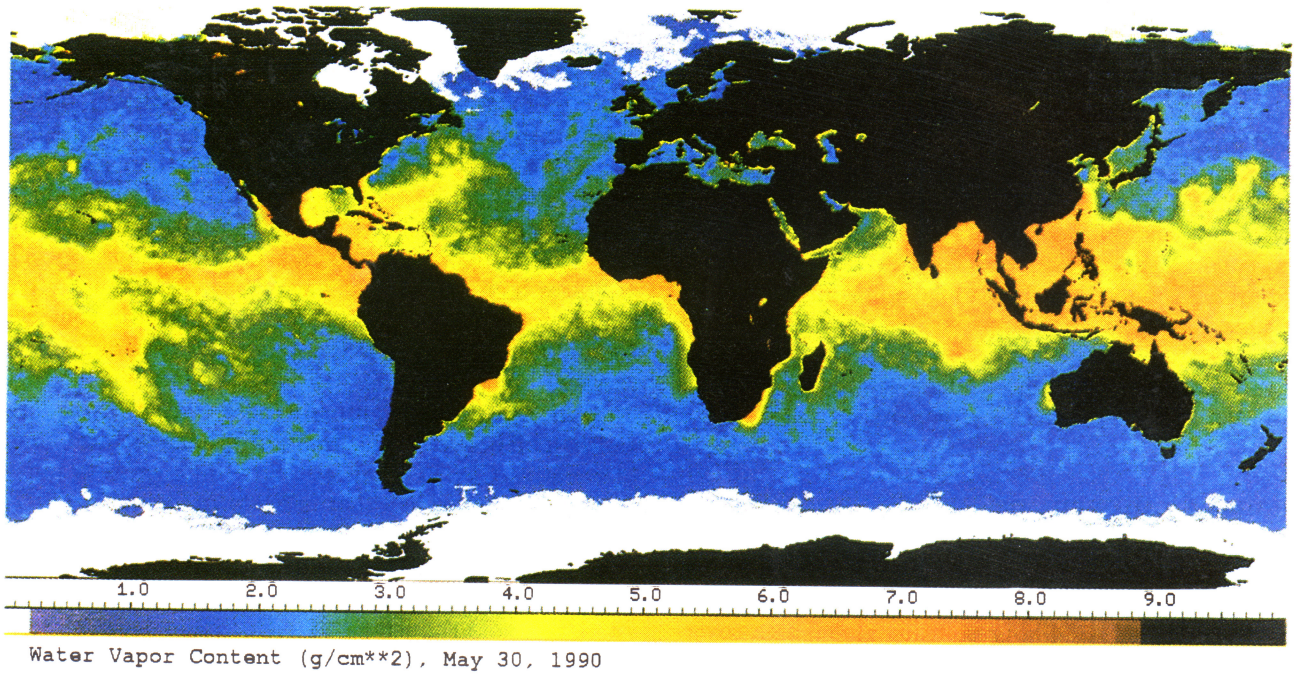

Plate 7b. Global atmospheric water vapor (grams per square centimeter) computed from SSM/I data for the week May 27 to June 2, 1990.

in the northern subpolar latitudes than in the southern ocean. At midlatitudes the two methods are very similar with average differences very near zero. Comparing water vapor and $T_4 - T_5$ temperatures differences (Appendix B) shows that for this summer period the infrared channel temperature difference is not a function of atmospheric moisture for latitudes above 20°N. This is in contrast to the atmospheric simulations (Appendix B) which suggest a linear dependence of water vapor on the $T_4 - T_5$ difference.

Viewing the temperature difference maps as histograms, the WVSST-quadratic SST differences in Figure 7a have a peak value of about -0.2 K with a tail toward positive differences. The negative peak value is due to the overestimation by the quadratic SST in the low moisture regions of the higher latitudes. As seen

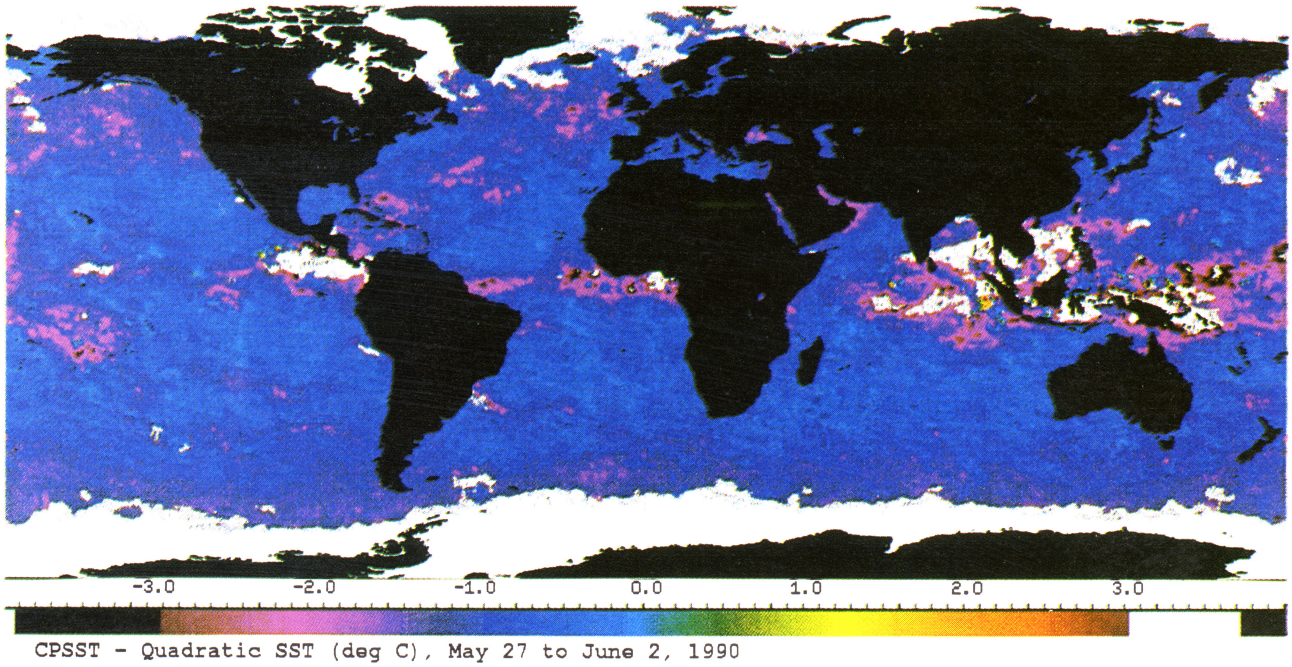

Plate 7c. Global temperature difference (degrees Celsius) between the CPSST and the quadratic SST (CPSST-quadratic) for May 27 to June 2, 1990.

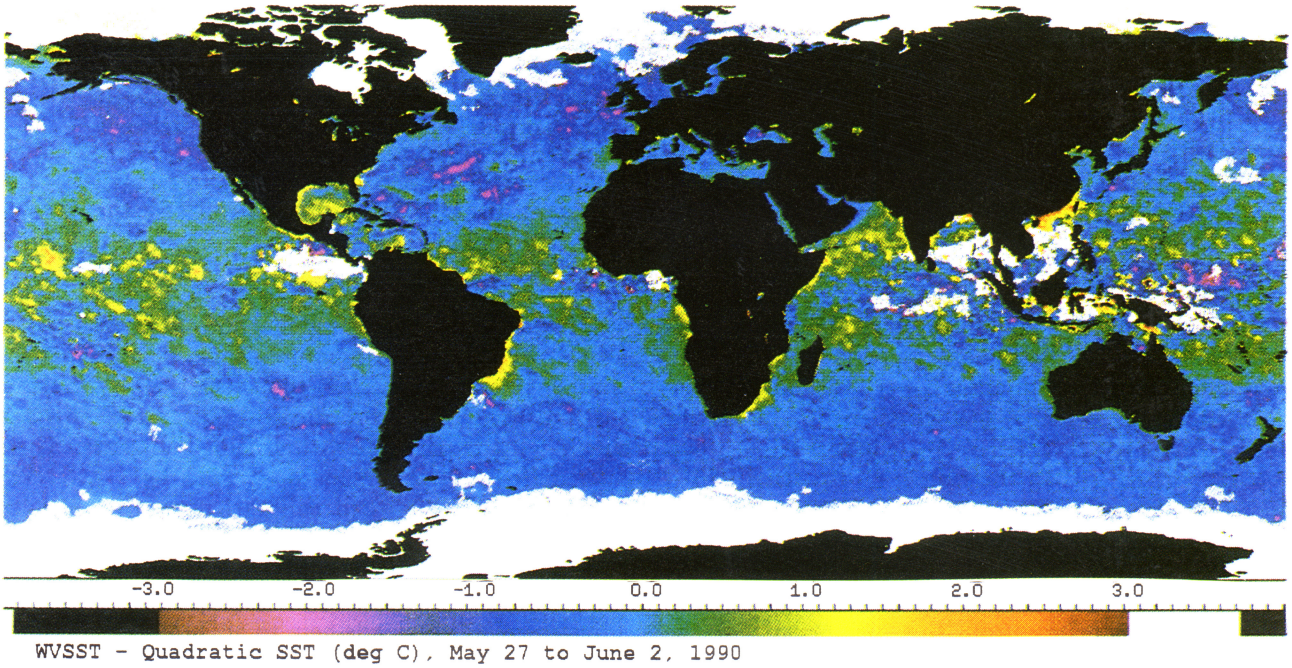

Plate 7d. Global temperature difference (degrees Celsius) between the WVSST and the quadratic SST (WVSST - quadratic) for May 27 to June 2, 1990.

in Appendix B these overestimates are due to the similar range of the $T_4 - T_5$ temperature differences in the low atmospheric moisture subpolar region as were found in the midlatitudes. This becomes an overestimate for the low-moisture content of the higher latitudes. The positive tail of the distribution is caused by the lower latitude underestimates of the quadratic SST compared with the WVSST. The wide range of positive values represented by this tail was not clear in the difference map of Plate 7d. The histogram mean of -0.21 K exhibits the strong influence of this positive tail on the overall distribution. In addition, the large RMS difference of 1.13 K is due to the spread of this tail.

The difference histogram between the CPSST and the WVSST (Figure 7b) is dominated by negative values with a mean difference of -1.13 K and an RMS of 1.44 K.

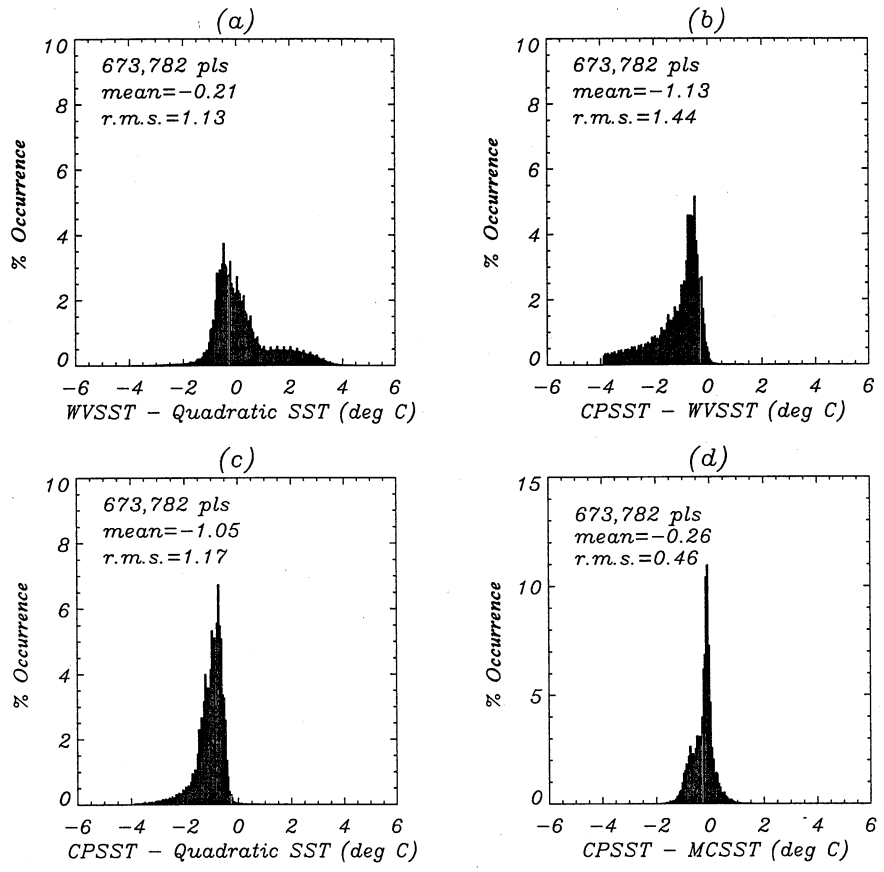

Figure 7. (a) Histogram of the temperature differences between the WVSST and the quadratic SST for the week May 27 to June 2, 1990. (b) Histogram of the temperature differences between the CPSST and the WVSST for the week May 27 to June 2, 1990. (c) Histogram of the temperature differences between the CPSST and the quadratic SST for the week May 27 to June 2, 1990. (d) Histogram of the temperature differences between the CPSST and the MCSST for the week May 27 to June 2, 1990.

These negative values are all due to the underestimates of the CPSST in the high-moisture regions of the tropical oceans and surrounding the lower-latitude continental boundaries. A similar histogram was found for the CPSST-quadratic SST (Plate 7c) which is slightly less negatively skewed than the histogram for the CPSST-WVSST differences (Figure 7b). The mean difference of -1.05 K is smaller than that for the WVSST as is the RMS difference of 1.17 K. Without looking at the spatial distributions of the differences in Plates 7c and 7d one might conclude from this histogram that the quadratic SST performs better when compared with the CPSST.

Finally, the difference histogram between the CPSST and the MCSST (Figure 7d) is as expected almost centered about zero. The large peak at 0.0 K indicates the similarity between the two algorithms in terms of the atmospheric moisture correction. The slight bias to the negative indicates that MCSST often overestimates the CPSST.

Buoy Comparisons

Since drifting buoy data have become the standard reference by which satellite SST algorithms are judged, we decided to compare our global SST maps with coincident drifting buoy SST measurements. This comparison is made in spite of the fact that both the WVSST and the quadratic SST are both skin SST algorithms and should not compare well with drifting buoy data. These buoy data were the "superobs" used by CAC NWS for the computation and calibration of their blended SST product [*Reynolds*, 1988]. These data are collected over the Global Telecommunications System (GTS) and comprise a wide variety of buoy and sensor types. No adjustment will be made here to account for individual differences between buoys and buoy SST sensors. All of the buoy measurements were treated equally in developing an SST data set to compare with the satellite SSTs.

A histogram of the WVSST - buoy SST differences (Figure 8a) contains a large peak at 0.0 with a mean of -0.34 K and a skewness toward negative differences. The equivalent histogram for the CPSST (Figure 8b) also has its peak located at 0.0 K with a much stronger bias to the negative difference side of the histogram. The mean value of -1.07 K clearly indicates this offset compared to the mean value of -0.34 K for the WVSST differences. The mean of the quadratic SST (Figure 8c) difference (-0.29 K) is slightly less than that for the

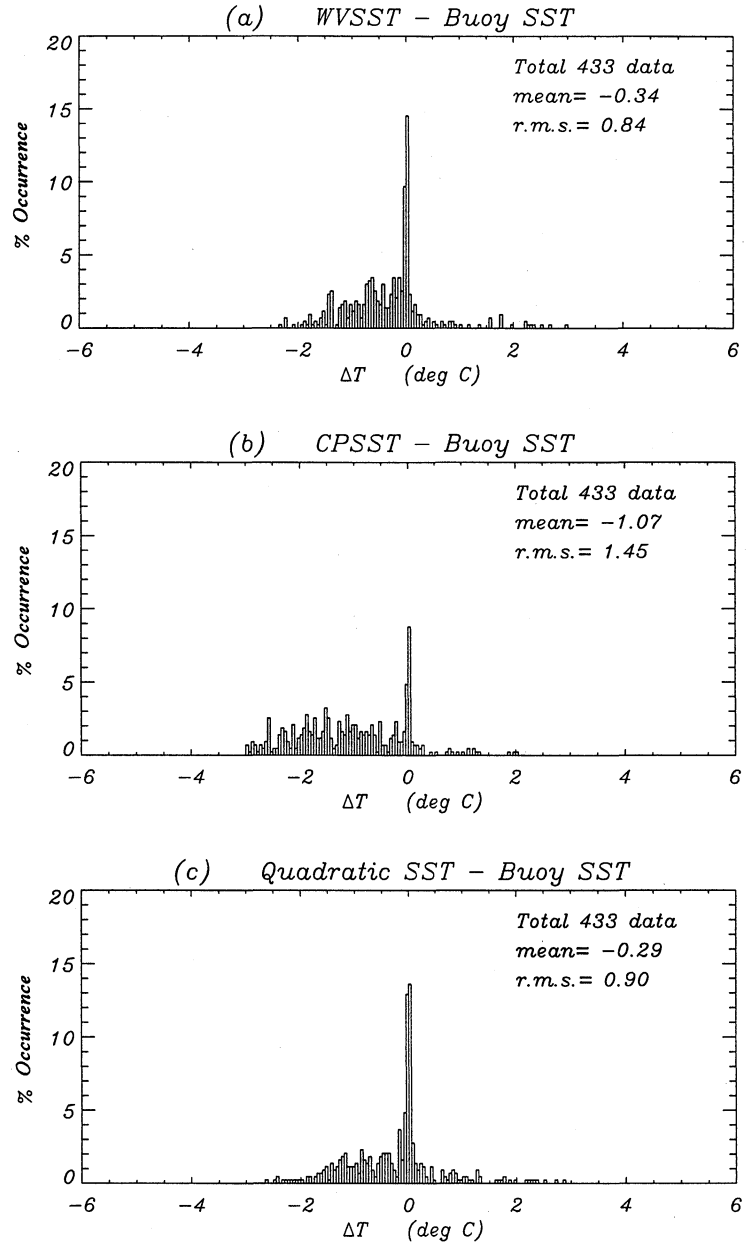

Figure 8. (a) Histogram of the global temperature differences between the WVSST and drifting buoy SSTs for May 27 to June 2, 1990. (b) Histogram of the global temperature differences between the CPSST and drifting buoy SSTs for May 27 to June 2, 1990. (c) Histogram of the global temperature differences between the quadratic SST and drifting buoy SSTs for May 27 to June 2, 1990.

WVSST, while the RMS for the quadratic SST (0.90 K) is a bit larger than that for the WVSST (0.84 K). Thus against drifting buoy data these two algorithms appear to perform equally well if one only considers the histogram comparison. The difference maps demonstrate that there is a slight difference with the quadratic SST underestimating the WVSST (and the buoy SST) in the tropics and overestimating the WVSST and the buoy values at higher, polar latitudes.

Discussion

The goal of this study is to examine possible correction of infrared SST estimation for the known contamination due to atmospheric water vapor. In this case we have used independent microwave measurements of atmospheric water vapor from the SSM/I to provide correction for the AVHRR skin SST algorithm. Thus we have used two thermal infrared channels from the AVHRR and an independent atmospheric moisture estimate as our three independent pieces of information for the water vapor corrected infrared SST (WVSST) computation.

We evaluated the performance of the WVSST against a similar approach using the square of the difference between the two thermal infrared channels to estimate the water vapor correction (the quadratic SST). Atmospheric simulations and comparisons with in situ skin

and bulk SST measurements showed the two algorithms to have similar statistics with the WVSST generally performing slightly better than the quadratic SST. In almost all cases, both new algorithms produced smaller errors (in terms of in situ minus satellite SST differences) than the MCSST and CPSST algorithms. Comparisons of SST patterns for an AVHRR image from the South Pacific revealed that the CPSST-WVSST differences matched that of atmospheric moisture, while the CPSST-quadratic SST differences did not. Applied to global AVHRR data, the quadratic SST method overestimated the WVSST at high latitudes and underestimated the WVSST at tropical latitudes. Comparing the core of the quadratic SST method (the $T_4 - T_5$ temperature difference) with coincident atmospheric water vapor (Appendix B) demonstrated that this temperature difference is not a function of water vapor for midlatitudes and high latitudes. In the tropics this temperature difference does correlate with atmospheric moisture but with a fairly wide spread that leads to the underestimates of WVSST. Overall, the WVSST appeared to give the best results for the widest range of conditions.

These patterns held true for both individual AVHRR images from the South Pacific and for a week long composite of global AVHRR data. Thus the results do not appear to be a function of time or space scale. The fact that the WVSST compares best with week-long buoy SSTs was a real surprise since this new SST algorithm is designed for satellite skin and not buoy SST. This significant similarity between the WVSST and the coincident buoy SST data indicates the importance of the water vapor correction over that of the skin versus bulk temperature. It is encouraging that the quadratic SST method performs nearly as well as the WVSST when compared with the buoy data. Thus for those periods of time where no SSM/I data are available, the quadratic formulation can be used to compute SST from the AVHRR data. After July 1987, when the SSM/I data became available, the WVSST algorithm should be used to compute SST from the AVHRR and other infrared satellite imagery. It is unclear as to why the CPSST performed so poorly in this comparison with drifting buoy data since its operational coefficients are derived from similar buoy SST matchups.

Conclusions

The significant conclusion here is that independent microwave measurements of atmospheric water vapor can be used to correct infrared estimates of SST. This is very encouraging for future satellite sensors that plan to use microwave radiometers to correct infrared temperature measurements. For the present a combination of water vapor computed from the SSM/I and the infrared radiances from the AVHRR can be used to accurately compute SST. Both global and single image patterns of atmospheric moisture appear very similar to the SST corrections provided by the WVSST as judged against the earlier CPSST and MCSST algorithms. While the WVSST algorithm was developed for skin SST, it appears to produce a most accurate bulk temperature when compared with drifting buoy and ship-based bulk SST measurements.

When SSM/I data are not available, a formulation that adds a quadratic term (square of the two thermal infrared channel temperature differences) performs almost as well as the WVSST at least for the high-moisture region of the tropics. This is a problem at the very low moisture contents of the high latitudes where the quadratic SST is consistently too high. This is most noticeable in that the differences between the quadratic SST and the CPSST do not follow the water vapor patterns.

In future studies we hope to be able to understand the relationship between atmospheric water vapor content and the $T_4 - T_5$ temperature difference. We also plan to determine the added influence of atmospheric aerosols on the computation of satellite SST. It is well know that major aerosol loadings from active volcanoes markedly affect the infrared SST, but there is no systematic correction procedure presently in place. We hope to develop a procedure that can be systematically used to correct SST for skin, water vapor, and aerosol effects.

Appendix A

The transmissivity of the atmosphere in the infrared can be written as

$$\tau_i = e^{-k_i u} \tag{A1}$$

where k_i is the absorption coefficient and u is the absorption. The subscript i represents the different measurement channels (i.e., wavelengths). If $k_i u$ is small, as we expand to the second order, equation (A1) becomes

$$\tau_i = 1 - k_i u + \frac{(k_i u)^2}{2} \tag{A2}$$

Recalling that the coefficient of the infrared channel temperature difference is written as

$$\gamma = \frac{1 - \tau_4}{\tau_4 - \tau_5} \tag{A3}$$

we can rewrite this using (A2) as

$$\gamma = \frac{k_4 - k_4^2 u/2}{k_5 - k_4 - (k_5^2 - k_4^2)u/2} \tag{A4}$$

This can be rewritten as

$$\gamma = \frac{k_4 - k_4^2 u/2}{k_5 - k_4}\left[\frac{1}{1 - (k_5 + k_4)u/2}\right] \tag{A5}$$

Now because $k_i u$ $(i = 4, 5)$ is small, this equation approaches

$$\gamma = \frac{k_4 - k_4^2 u/2}{k_5 - k_4}[1 + (k_5 + k_4)u/2] \tag{A6}$$

We now neglect the $k_i^3 u^2$ term and find that

$$\gamma = a_3' + a_4 u \tag{A7}$$

where

$$a_3' = \frac{k_4}{k_5 - k_4} \tag{A8}$$

and

$$a_4 = \frac{k_4 k_5/2}{k_5 - k_4} \tag{A9}$$

Appendix B

In order to better understand the differences between the WVSST and the quadratic SST we decided to compare the input data for the computation of these differences. We first used our simulation data set and radiative transfer code to compute the correlations between the $T_4 - T_5$ temperature differences and the water vapor contents from the radiosonde profiles. The results in Figure B1a show a quasi-linear relationship with larger

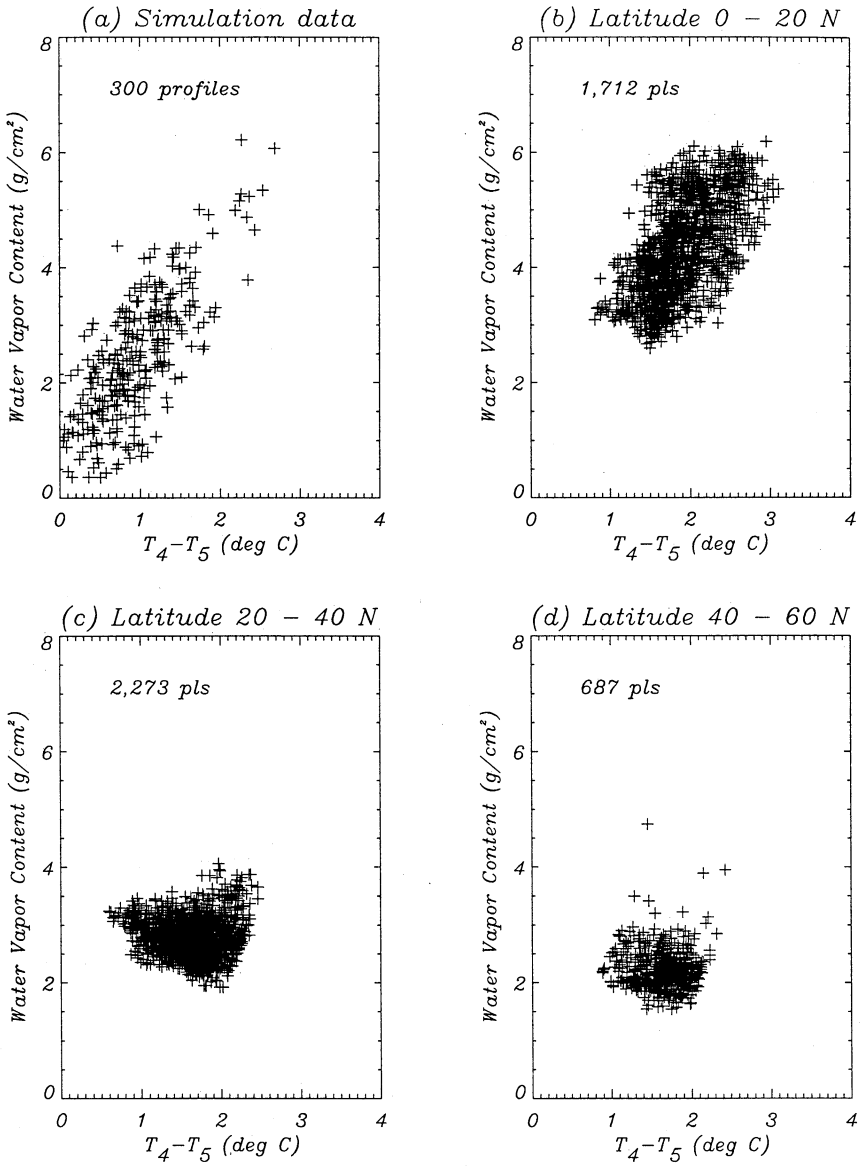

Figure B1. (a) Scatter diagram of the relationship between integrated atmospheric water vapor and $T_4 - T_5$ using the simulation database and radiative model. (b) Scatter diagram of the relationship between 2-day SSM/I water vapor contents and $T_4 - T_5$ from the GAC AVHRR data for the North Pacific (130°W to 180°W) for the latitudes between 0 and 20°N. (c) Scatter diagram of the relationship between 2-day SSM/I water vapor contents and $T_4 - T_5$ from the GAC AVHRR data for the North Pacific (130°W to 180°W) for the latitudes between 20 and 40°N. (d) Scatter diagram of the relationship between 2-day SSM/I water vapor contents and $T_4 - T_5$ from the GAC AVHRR data for the North Pacific (130°W to 180°W) for the latitudes between 40 and 60°N.

values of $T_4 - T_5$ being associated with higher water vapor contents. This is consistent with the traditional assumption that the $T_4 - T_5$ difference is related to atmospheric moisture. There is a slight bias of this relationship towards higher moisture contents. Nevertheless this linear result was not consistent with the over and under SST estimates by the quadratic SST algorithm.

Turning to real AVHRR data, we used the data for the global comparison differences between the WVSST and the quadratic SST. We compared the $T_4 - T_5$ temperature differences with the nearly coincident SSM/I derived atmospheric moisture contents. Data between 130° and 180°W and from 0 to 60°N were used to compute the water vapor from 2 days of SSM/I data surrounding each day from which we took the $T_4 - T_5$ differences. We did this for two different days of $T_4 - T_5$ differences to increase our statistical sample size. Correlations computed for 20° latitude zonal bands provided some surprising results (Figures B1b-B1d). The lowest latitudes (0−20°N, Figure B1b) showed a linear dependence of water vapor on the $T_4 - T_5$ difference for water vapor values above about 2.5 g/cm^2.

The other two zonal bands (Figures B1c and B1d) did not, however, show any relationship between the $T_4 - T_5$ difference and atmospheric moisture. Water vapor amounts were lower for the highest latitude band (40 − 60°N, Figure B1d), while the midlatitude moisture values were a bit higher (Figure B1c). Both plots, however, had the same range of $T_4 - T_5$ values for almost constant water vapor amounts. The fact that this range is the same for both regions is the reason why the quadratic SST overestimates the WVSST for the high latitudes where the water vapor amounts are low. It is not at all clear why both of these zonal bands do not show the linear dependence of atmospheric moisture on the $T_4 - T_5$ difference that appears for the atmospheric simulations (Figure B1a). We plan to further investigate this relationship by studying seasonal and latitudinal relationships between $T_4 - T_5$ and atmospheric water vapor.

Acknowledgments. This research was sponsored by the National Aeronautics and Space Administration (NASA) as part of the Earth Science Division (Code Y) under its program in earth science and modeling. Many thanks go to the two different program managers (Bill Patzert and Mike van Woert) for their continuing interest and support of this research effort. During this study Y. Yu was on leave from the Ocean University of Qingdao, China, and we are grateful to his university for granting this leave. Ian Barton graciously allowed us to use his atmospheric simulation code and also contributed valuable suggestions as one of the reviewers of an earlier version of the paper. The inclusion of the quadratic SST comparisons were suggested by Ian. We are also very grateful to an anonymous reviewer who suggested changes in our derivation of the WVSST algorithm. The suggestion was to build on previous work and that led to our starting here with equation (1). We added Appendix A to more completely document this derivation and again are grateful to the reviewer for pointing out this approach.

References

Barton, I.J., Transmission model and ground-truth investigation of satellite-derived sea surface temperatures, *J. Clim. Appl. Meteorol., 24,* 508-516, 1985.

Brown, J.W., O.B. Brown, and R.H. Evans, Calibration of advanced very high resolution radiometer infrared channels: A new approach to nonlinear correction, *J. Geophys. Res., 98,* 18,257-18,268, 1993.

Brown, O.B., J.W. Brown, and R.H. Evans, Calibration of advanced very high resolution radiometer infrared observations, *J. Geopys. Res., 90,* 11,667-11,677, 1985.

Emery, W.J., G.H. Born, D.G. Baldwin, and C.L. Norris, Satellite-derived water vapor corrections for Geosat altimetry, *J. Geophys. Res., 95,* 2953-2964, 1990.

Hagan, D.E., A basic limitation of the split window method for SST retrievals when applied to a wide range of water vapor conditions, *Geophys. Res. Lett., 16,* 815-817, 1989.

Harris, A.R., and I.M. Mason, An extension to the "split-window" technique giving improved atmospheric correction and total water vapor, *Int. J. Remote Sens., 13,* 881-892, 1992.

Kidwell, K.B., NOAA polar orbiter data users guide, NOAA national environmental satellite, data, and information service, Washington, D.C., 1991.

Maul, G.A., and M. Sidran, Atmospheric effects on ocean surface temperature sensing from the NOAA satellite scanning radiometer, *J. Geophys. Res., 78,* 1909-1916, 1973.

McClain, E.P., W.G. Pichel, and C.C. Walton, Comparative performance of AVHRR-based multichannel sea surface temperatures, *J. Geophys. Res., 90,* 11,587-11,601, 1985.

McMillin, L.M., and D.S. Crosby, Theory and validation of the multiple-window sea surface temperature technique, *J. Geophys. Res., 89,* 3655-3661, 1984.

Reynolds, R.W., A real-time global sea surface temperature analysis, *J. Clim., 1,* 75-86, 1988.

Schluessel, P. and W.J. Emery, Atmospheric water vapor over oceans from SSM/I measurements, *Int. J. Remote Sens., 11,* 753-766, 1990.

Schluessel, P., H.-Y. Shin, W.J. Emery, and H. Grassl, Comparison of satellite-derived sea surface temperatures with in situ skin measurements, *J. Geophys. Res., 92,* 2859-2874, 1987.

Schluessel, P., W.J. Emery, H. Grassl, and T. Mammen, On the bulk-skin temperature difference and its impact on satellite remote sensing of sea surface temperature, *J. Geophys. Res., 95,* 13,341-13,356, 1990.

Walton, C.C., Nonlinear multichannel algorithm for estimating sea surface temperature with AVHRR satellite data, *J. Appl. Meteor., 27,* 115-124, 1988.

Walton, C.C., E.P. McClain, and J.F. Sapper, Recent changes in satellite-based multichannel sea surface temperature algorithms, *Rep. MTS 90,* Mar. Technol. Soc., Washington, D.C., Sept., 1990.

Wick, G.A., W.J. Emery, and P. Schluessel, A comprehensive comparison between satellite measured skin and multichannel sea surface temperature, *J. Geophys. Res., 97,* 5569-5595, 1992.

W. J. Emery, G. A. Wick, and Y. Yu, CCAR Box 431, University of Colorado, Boulder, CO 80309.

R. W. Reynolds, Climate Analysis Center, National Weather Service, World Weather Building, Washington, DC 20233

P. Schluessel, Meteorologisches Institut, Universitat Hamburg, Bundestr, 55, 2000 Hamburg, Germany

(Received August 30, 1993; revised November 12, 1993; accepted November 12, 1993.)